Paper accepted for publication in Transportation Geotechnics, 10 February 2020
DOI: 10.1016/j.trgeo.2020.100335

The shadow effect on the ground surface due to vibration transmission from a railway tunnel

Qiyun Jin*, David J. Thompson, Daniel E.J. Lurcock, Evangelos Ntotsios

Institute of Sound and Vibration Research, University of Southampton, Southampton SO17 1BJ, UK

*: corresponding author, email: q.jin.2017@gmail.com

Abstract. The prediction of the ground vibration transmitted from tunnels to neighbouring buildings is a vital step in the assessment of the ground-borne noise in buildings. In empirical models it is commonly assumed that the level of ground vibration reduces monotonically with the distance away from the tunnel alignment. In reality, a 'shadow' zone is observed above the tunnel. This is first illustrated using measurements made above an operational railway line. To understand and characterise this effect, a study has then been carried out using various simulation models. Using an analytical model for the response to a point force acting in a homogeneous full-space, it is shown that the response is principally in the form of shear waves which radiate to the side rather than compressional waves which radiate in the direction of the load. This leads to a 'shadow' zone forming above a certain frequency, even in the absence of a tunnel and the absence of a free ground surface. The ground surface is next introduced by considering the response of a half-space to a point force, using a semi-analytical model. This is shown to exhibit similar behaviour although with differences caused by the free ground surface. Finally, a numerical 2.5-dimensional finite element / boundary element model is used to determine the response of a half-space ground to a force acting at the bottom of a concrete tunnel. The extent of the shadow is defined as the width to the point of maximum response. This depends largely on the depth of the excitation force and the shear wave speed of the soil. Although similar features are found with or without the tunnel, the presence of the tunnel structure causes a reduction in the shadow width, and the level difference within the shadow region is slightly increased. A tunnel with a smaller diameter leads to an increase in the frequency at which a given shadow effect occurs, but the tunnel lining thickness has negligible influence. The existence of shadow effect should be taken into account when making predictions of ground vibration using empirical models.

Keywords: railway ground vibration, tunnel/ground model, transfer mobility, 2.5D finite element / boundary element method

1 Introduction

Ground-borne noise is one of the most important environmental issues related to underground transit systems, especially in busy urban areas. The prediction of the ground vibration transmitted from tunnels to the ground surface is a vital step in the assessment of the ground-borne noise in buildings. It is often assumed that the level of ground vibration reduces monotonically with the distance away from the tunnel alignment. In reality, a region with lower vibration amplitudes is often observed directly above the tunnel, which is sometimes referred to as a 'shadow' zone. Although the area of most interest is usually located away from the alignment, pressure on land use means construction close to or even above railway alignments is now commonplace.

Recent reviews of ground vibration from trains have been presented for example by Lombaert et al. [1] and Thompson et al. [2]. Connolly et al. [3] gave an overview of the scale of the problem of ground vibration by reviewing reports covering commercial vibration assessments undertaken at 1604 locations. Sheng [4] gave a review of modelling approaches used for the vibration generated by trains in tunnels. These can be numerical, e.g. using finite elements, boundary elements, finite difference etc., analytical, semi-analytical or empirical.

An early review of models and measurements of the propagation of vibration through the ground was given by Gutowski and Dym [5]. They separated the attenuation with distance into two terms, one due to geometric attenuation, which depends on the wave type, and a second due to damping. This can be written as [6]:

$$A(d) / A_0 = (d/d_0)^{-\alpha} \times \mathrm{e}^{-\beta(d-d0)} \quad (1)$$

where $A(d)$ is the amplitude at distance d and A_0 is the amplitude at a reference point d_0. For example, geometric spreading from a point source on the ground surface can be assumed to correspond to $\alpha = ½$, while for a point source at some depth $\alpha = 1$. Other coefficients are given by Gutowski and Dym [5] for line sources. The effect of damping, β, has to be determined for the site in question and depends on frequency. Attenuation laws of the form $d^{-\alpha}$ are used for example by Kuppelwieser and Ziegler [7] and Madshus et al. [8] in their empirical calculation schemes.

Hood et al. [9] proposed an empirical calculation procedure for both ground-borne noise and feelable vibration. For feelable vibration the amplitude was found to depend on radial

distance R (in m) according to $(R/10)^{-0.97}$. For ground-borne noise the propagation with distance (expressed in decibels) was given by:

$$B + C.\log_{10}((x+10)/10) + D.\log_{10}(Z/R_0) + E.\log_{10}(W/10) \quad (2)$$

where B, C, D, E were determined from multiple regression analysis for each frequency band. x is the horizontal distance from the tunnel (in m), Z is the tunnel depth (in m), W is the tunnel width (in m) and R_0 is a constant. The results were found to be independent of soil lithology. In the empirical approach proposed by the US Federal Transit Administration [10] the propagation is based entirely on measurements.

Forrest and Hunt [11, 12] developed an analytical model of a tunnel in a full-space ground, later called 'pipe-in-pipe', and showed example results at different distances as a function of angle around the tunnel. Kuo et al. [13] extended this model to study parallel twin tunnels in a full-space. Contour plots were presented of vibration amplitude in the plane containing the cross-section of the tunnel. Sheng et al. [14] developed analytical models for a circular tunnel in a layered ground based on a discrete wavenumber approach. Some example results were presented at two frequencies. It was concluded that a lined tunnel may reduce the responses at the ground surface immediately above the tunnel compared with an unlined tunnel.

Jones et al. [15] used a two-dimensional coupled finite element / boundary element (FE-BE) method to study the vibration due to tunnels. They showed that the vibration decays with lateral distance beyond about 20 m but, closer to the tunnel alignment, the vibration behaviour is more complex. Comparisons were also made between lined and unlined tunnels. Their results were for a single relatively stiff soil type. In order to take account of both vertical and lateral vibration a 'pseudo-resultant' was introduced.

Sheng et al [16] developed a wavenumber (i.e. 2.5-dimensional, 2.5D) FE-BE method and used it to compare a large single bore tunnel with smaller twin bore tunnels. Results at certain frequencies (20, 40, 80 and 160 Hz) were plotted for positions along the ground surface as part of this comparison. They noted that the vibration attenuation in the lateral direction was weaker than in the tunnel direction, especially at high frequencies. Moreover, the maximum response did not occur directly above the tunnel; the position of maximum response was found to move towards the tunnel as frequency increases.

Clouteau et al. [17] and Degrande et al. [18] modelled a tunnel in a layered soil using a periodic FE-BE approach and gave some examples of the response on the free surface at certain frequencies. Ding et al. [19] used this method to study the ground response above a metro tunnel at four distances (0, 20, 40 and 60 m) to the tunnel centreline. Gupta et al. [20] studied the effect of tunnel and soil properties on vibration from a tunnel using both the

periodic FE-BE approach and the analytical pipe-in-pipe approach. Results were shown at several different distances. The overall root-mean-square vibration due to a train was plotted against distance showing that the maximum value occurred away from the tunnel.

Yang and Hung [21] used a 2.5D finite element / infinite element approach to model the vibration from a tunnel. They included an analysis of the dependence of vibration on lateral distance for certain frequencies. Galvín et al. [22] used a 2.5D coupled FE-BE model to study trains running both on the surface and in tunnel. Response spectra at different locations were presented but the dependence on distance was not studied. Lopes et al. [23] studied the full transmission path from the tunnel to the building: the track–tunnel–ground system was modelled by a 2.5D FEM–Perfectly Matched Layer approach and the building by a 3D FEM method. No results were presented for the free ground responses as a function of distance.

As noted above, it is often considered in empirical models that the response on the ground surface decreases monotonically with the distance from the tunnel. However, although such an attenuation law can be used for surface trains, it has been seen that it may not be suitable for tunnel cases. The existence of a shadow zone makes it more difficult for empirical models to predict accurately the vibration of buildings located close to the tunnel. Although the shadow zone has been observed by some authors, e.g. [14, 15], no systematic analysis has been carried out.

The aim of this paper is to study the shadow zone phenomenon using both analytical and numerical models and to quantify its effect. In Section 2, a set of measurement data from a free-field site near a railway tunnel is presented to demonstrate the existence of the shadow zone. In Section 3, the response on the ground surface to the excitation in a tunnel is predicted by a 2.5D FE-BE model using in-house software WANDS [24]. Based on the prediction results, the ‘shadow effect’ is defined in terms of three basic parameters. This is used to describe the fact that the vibration levels within an area above the tunnel are lower than those further away from the centreline at some frequencies. The mechanism behind this phenomenon is explained using results for a full-space in Section 4. The characteristics of the shadow area are analysed in Section 5 using a semi-analytical half-space ground model, showing that the so-called shadow zone exists regardless of the tunnel structure. However, the tunnel structure will affect the extent of this irregular distribution, so this influence is analysed in a parametric study in Section 6 based on the 2.5D FE-BE model. Some preliminary results from this study were presented by Jin and Thompson [25].

2 Observation from experimental data

2.1 Description of the measurement data

In this section, results are presented from measurements carried out to demonstrate the presence of the shadow effect. It is much more difficult to perform measurements in an urban environment, due to the presence of many buildings as well as background vibration caused by traffic, etc. Therefore, the measurements were taken at a free-field location above a tunnel on the high-speed line HS1 at Hollingbourne, Kent, UK. The tunnel, as shown and illustrated in Figure 1, was constructed as a cut-and-cover tunnel of length 170 m using precast concrete arch segments of thickness 325 mm. The double-track tunnel has a height of 8.5 m and a width of 14 m. The ground surface is approximately 15 m above the rail height. The soil properties here are unknown.

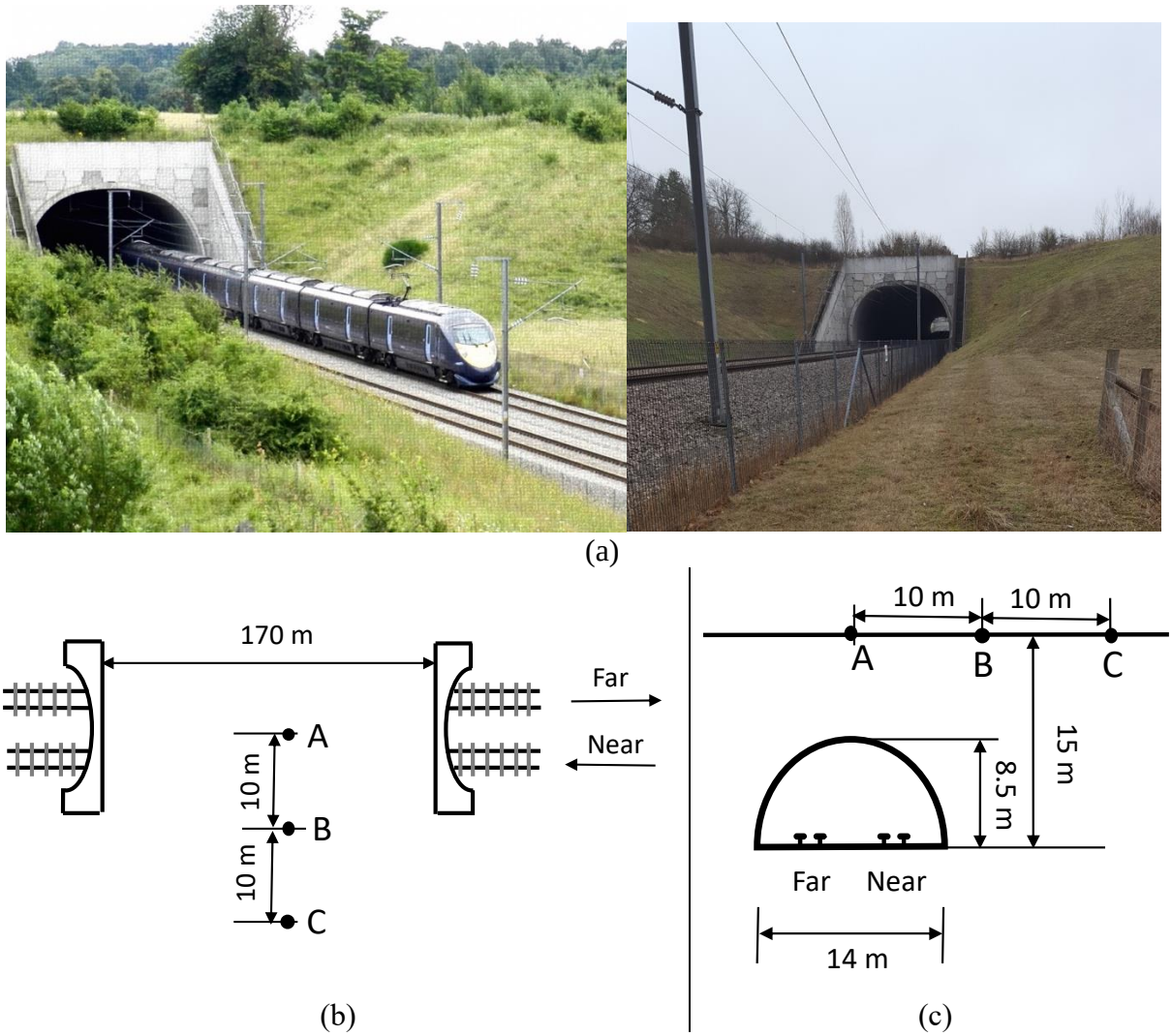

Figure 1. Photograph of the measurement site (a) and diagram of the measurement site (not to scale): (b) plan view (c) cross-section view

Vibration was measured on the ground surface above the tunnel during the passage of three types of trains: Javelin Class 395, Eurostar Class 373 and Velaro Class 374. The line speed at the location is 300 km/h (83.3 m/s); however, the maximum speed of the Class 395 trains is 225 km/h (62.5 m/s). The train speeds were close to these values and were similar in both directions. A total of 18 train passages were recorded, as listed in Table 1.

Table 1. Numbers of trains recorded in each direction

	Javelin Class 395	Eurostar Class 373	Velaro Class 374	Total
Far track	5	2	2	9
Near track	6	2	1	9

The vertical acceleration was measured using accelerometers with sensitivity 10 V/g and mass 0.64 kg mounted on a square aluminium mounting plate of length 150 mm and mass 0.3 kg. A small area of turf was removed and the plate was embedded in a thin layer of sand.

The vertical acceleration level was measured at three positions, marked A, B and C in Figure 1, when the trains passed in both directions; the two tracks are identified as ‘near’ (towards London) and ‘far’ (away from London). Point A was directly above the tunnel, while B and C were 10 and 20 m from the tunnel centreline.

2.2 Variation of vibration with distances

The results are given in one-third octave frequency bands, between 4 and 100 Hz. The acceleration levels in dB have been averaged over all train types for the measurements at each of the three locations. Results are shown in Figure 2 for trains on the far and near lines separately. The background noise is also shown indicating that sufficient signal-to-noise ratio is achieved over almost the whole frequency range.

It can be seen from Figure 2 that, for trains on both the far and near tracks, the vibration level below 10 Hz is highest at location A (above the tunnel alignment) and reduces with increasing distance (from location A to C). However, at higher frequencies the vibration levels at locations B and C are higher than at A for a broad range of frequencies. Thus, the maximum vibration level does not always occur directly above the tunnel.

The vibration levels at locations B and C are shown relative to those at A in Figure 3. The level difference between these locations has been determined for each train passage and the graph shows the mean and a range corresponding to +/- two standard deviations. Despite the variations among trains, the frequency range where the shadow effect appears can be clearly seen from Figure 3 as the range where the level difference is greater than zero. At location C

(at 20 m from the tunnel centreline) this occurs above about 16 Hz, for both far and near tracks, whereas at location B (at 10 m) it occurs above around 10 Hz. As seen in Figure 2, the vibration at C also exceeds that at B for frequencies above 20 Hz.

These results show the presence of the shadow effect qualitatively. In the remainder of the paper a more typical urban situation is considered using several different prediction models in an attempt to explain the phenomenon.

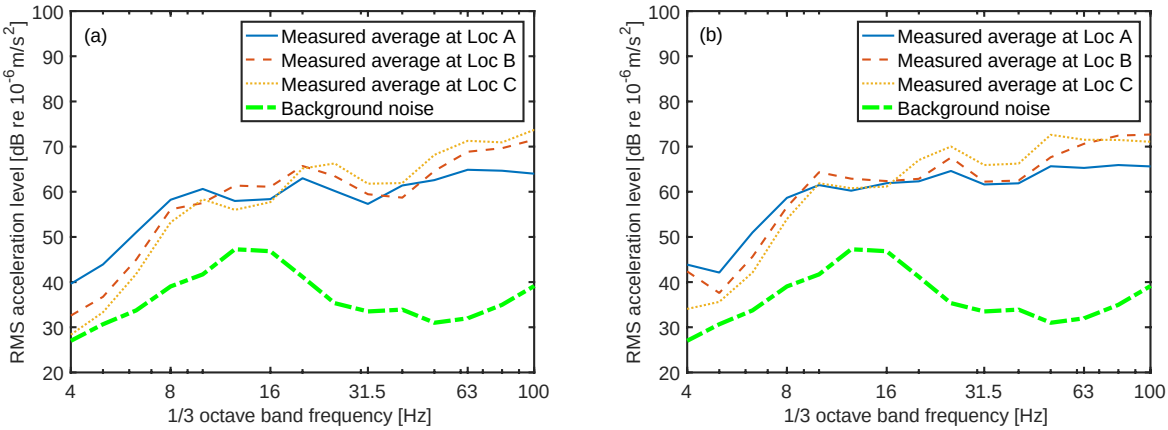

Figure 2. Averaged acceleration level and the background noise at different locations due to the trains on (a) far track; (b) near track. Locations A, B and C are at 0 m, 10 m and 20 m from the tunnel centreline respectively.

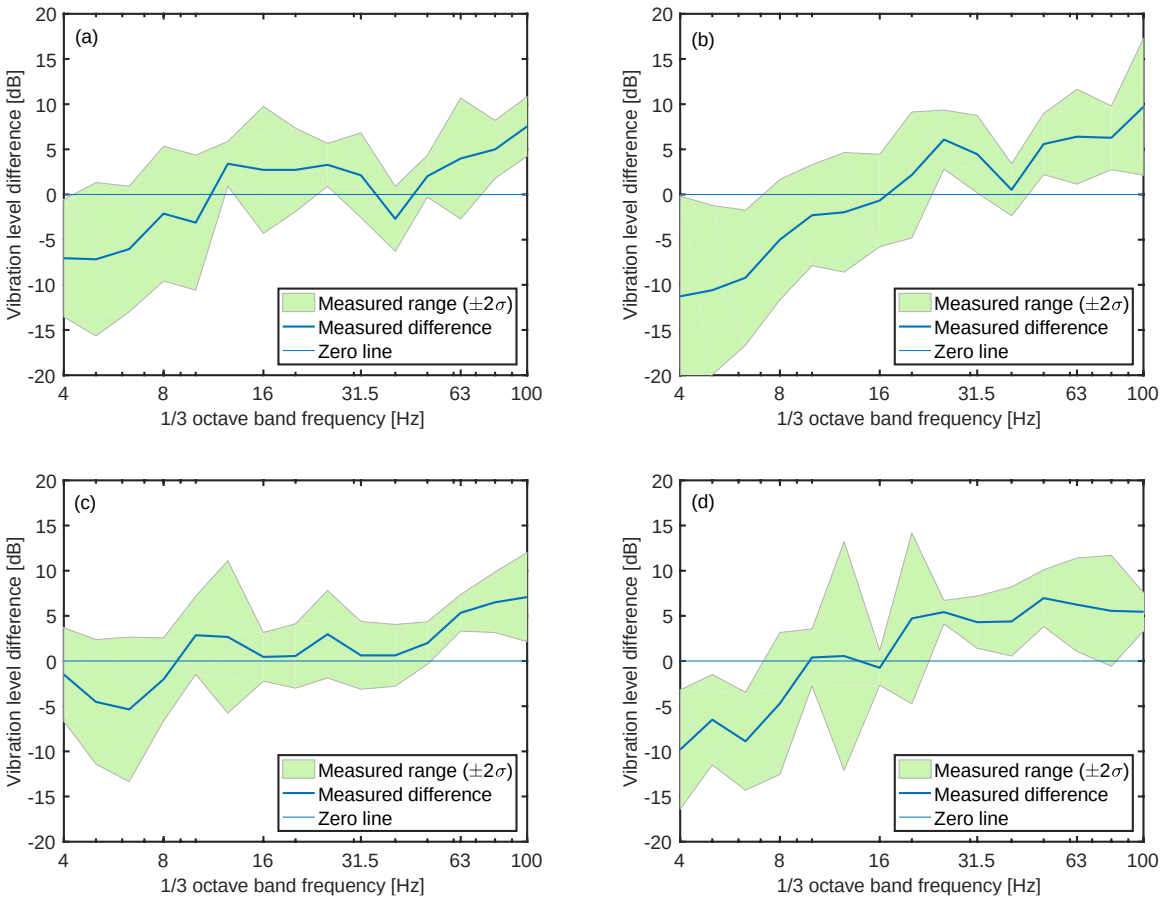

Figure 3. Vibration levels relative to location A. (a) B minus A for far track; (b) C minus A for far track; (c) B minus A for near track; (d) C minus A for near track.

3 Observation from simulation results

3.1 A 2.5D FE-BE tunnel/ground model

A study case is chosen based on a typical urban underground line with a concrete circular tunnel. This is represented in a numerical model, which is constructed using the wavenumber (2.5D) FE-BE method [16, 24]. A similar model can be found in Jin et al. [26]. The cross-section of the tunnel in the *y*-*z* plane is modelled with finite elements, whereas boundary elements are used for the ground including the free surface, as shown in Figure 4.

The geometry of the tunnel cross-section is modelled with 30, 8-node solid elements. The ground surface and the interface between the tunnel and soil are represented by 3-node boundary elements. The mesh of the ground surface extends to 30 m on each side of the tunnel centreline with a node spacing of 0.25 m. Unless otherwise stated, the depth from the ground surface to the tunnel centre is 15 m, and the inner and outer diameters of the tunnel are 3.81 m and 4.11 m respectively giving a wall thickness of 0.15 m. Figure 4 shows only part of the elements on the free surface and the tunnel depth is reduced to allow more details

to be visible in a compact figure. The track is omitted from the model for simplicity. A point force acts on the centre of the tunnel bottom. The assumed soil and tunnel material properties are given in Table 2. The soil represents London clay [18], with a value of compressional wave speed approximating saturated ground.

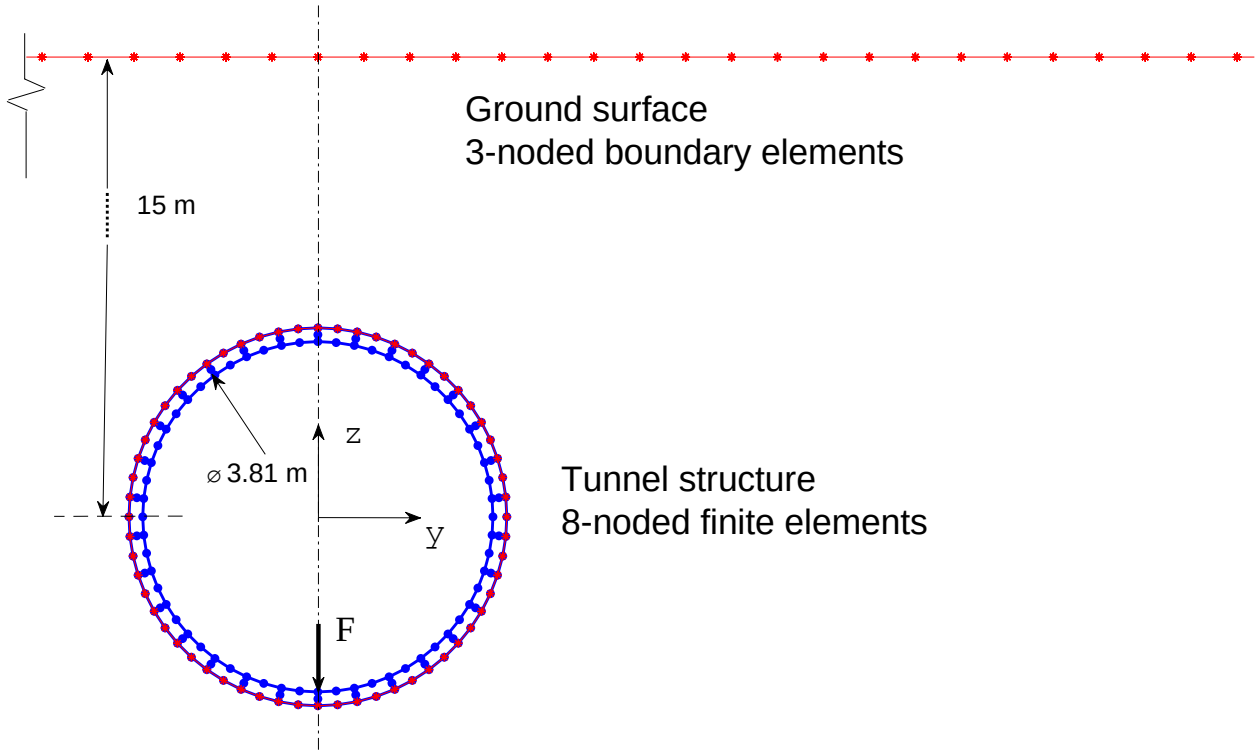

Figure 4. FE / BE mesh of the tunnel-ground cross-section.

Table 2. Material properties of the soil and tunnel used in the model [18].

Soil	S-wave speed	P-wave speed	Density	Loss factor
	220 m/s	1570 m/s	1980 kg/m^3	0.078
Concrete tunnel	Young's Modulus	Density	Poisson's ratio	Loss factor
	50 GPa	2500 kg/m^3	0.3	0.03

In the third direction (x) the geometry is assumed to be invariant. This is represented in the model in the wavenumber domain. The total number of wavenumbers calculated is 2048, with a linear spacing of 0.006 rad/m. The frequency range considered is from 1 to 100 Hz with 30 points per decade. The results are then converted to one-third octave bands by averaging the results for three frequencies per band.

3.2 Definition of shadow effect

Using the 2.5D FE / BE tunnel-ground model, the vertical displacements on the ground surface excited by a unit vertical force acting at the tunnel bottom are plotted in Figure 5(a), for some example frequency bands. The response is plotted in the same cross-section as the force, where x=0.

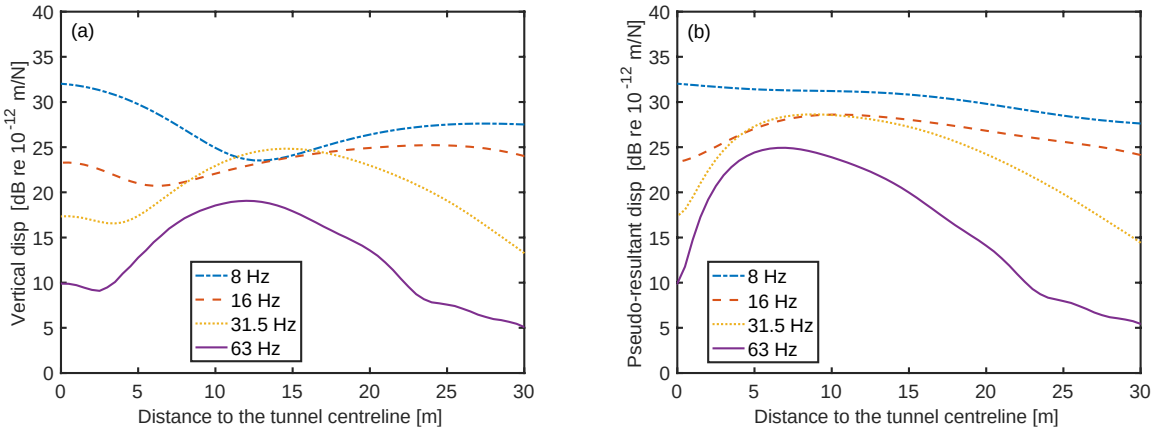

Figure 5. Response on the ground surface to a unit force at the tunnel base at different frequencies. (a) vertical response; (b) pseudo-resultant response

Depending on the frequency, the highest response levels are found at different distances from the tunnel. At 8 Hz, the maximum response occurs directly above the tunnel centreline. For frequencies above 16 Hz, however, the region of maximum response occurs at some distance away from the centreline and the response above the tunnel is up to 10 dB lower than the maximum level. This is consistent qualitatively with the experimental results shown in Section 2.

In addition, the pseudo-resultant responses are determined ($\sqrt{|u_y|^2 + |u_z|^2}$, with u_y and u_z the horizontal and vertical components of vibration, u_x is zero for x=0). These are shown in Figure 5(b). A similar phenomenon is seen here although the details are different. The distance where the maximum pseudo-resultant response occurs is closer to the centreline than that for the vertical response at the same frequency. The difference between the vibration levels is also larger, up to 15 dB.

3.3 Definition of parameters describing the shadow effect

Some parameters are introduced to quantify the characteristics of the shadow effect. Two of the example response curves shown in Figure 5(b) are replotted in Figure 6 to illustrate these. The dash-dot line shows the response at 8 Hz, while the solid line is the response at

63 Hz where the shadow area can be observed. Three important parameters are defined and illustrated in Figure 6 based on the result at 63 Hz.

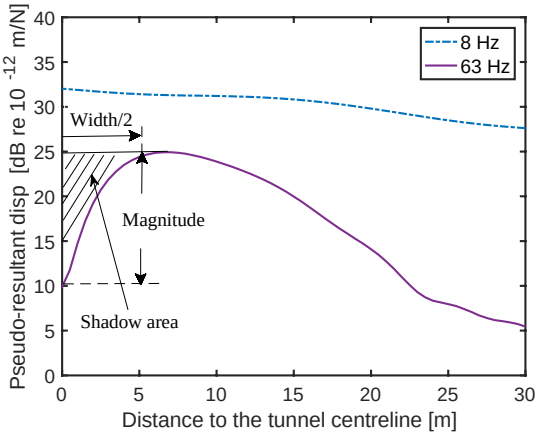

Figure 6. Vertical response on the ground surface in the *y* direction at different frequencies (*x*=0) showing the definition of the width and magnitude of the shadow zone.

First, the width of the shadow area is defined as twice the distance from the tunnel centreline to the position of maximum response. As seen in Figure 5, this width depends on the excitation frequency. Second, the magnitude of the shadow effect is identified as the difference (in decibels) between the maximum vibration level and that above the tunnel centreline at the same frequency. Third, the frequency above which the shadow effect can be observed is called the cut-on frequency. For frequencies above this (e.g. 16, 31.5 and 63 Hz in Figure 5) the maximum response is observed at some distance away from the tunnel centreline; below this frequency the magnitude and width of the shadow effect are both zero.

4 Exploration of mechanism using results from a full-space model

To assist in the interpretation of the shadow effect observed from the experimental data and the 2.5D tunnel-ground modelling results and to investigate the mechanism behind the phenomenon, results from a full-space are presented here. For a homogeneous full-space the vibration response can be determined analytically [27]. This will be used to show whether the same shadow phenomenon defined in Section 3 is also observed in the absence of both the tunnel structure and the ground surface. The role of the fundamental waves in forming the shadow area will be discussed.

4.1 Responses at a line above the excitation

For consistency with the 2.5D model, the horizontal axis is taken as *y* and vertical axis as *z*. A harmonic load is applied in the *z* direction. The ground parameters are the same as those

used for the tunnel case, as listed in Table 2. A different value of Poisson's ratio (0.33) is also chosen for comparison, while retaining the same shear modulus and therefore shear wave speed; the corresponding compressional wave speed is 440 m/s. The response is determined along a horizontal line of response points at a vertical height of 15 m above the forcing point. This is equivalent to the ground surface location in the previous section, except that in this full-space model there is no free surface.

Figure 7 shows examples at four frequencies for both values of Poisson's ratio. These are given in the form of the pseudo-resultant. The results are qualitatively similar to those in Figure 5. This shows clearly that a 'shadow effect' can occur in a full-space with no ground surface and no tunnel structure, especially for the ground with large Poisson's ratio.

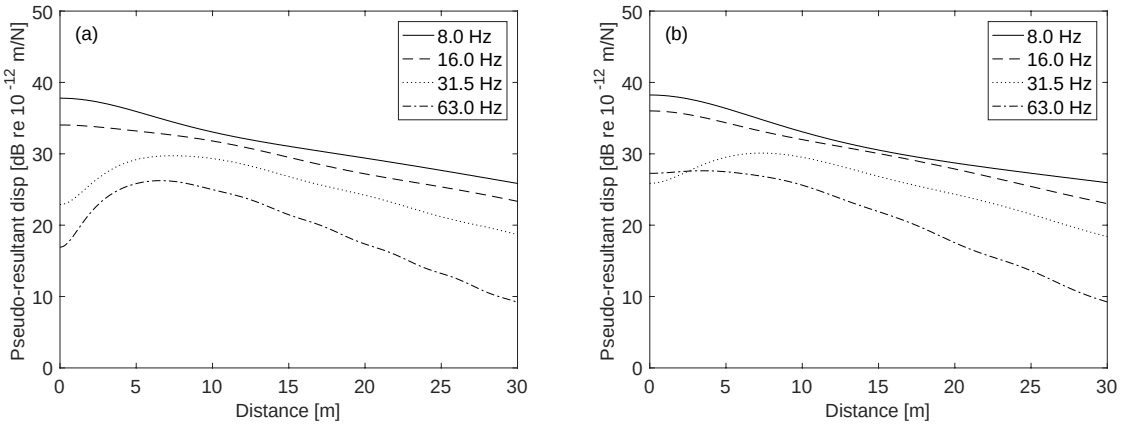

Figure 7. Pseudo-resultant for receivers on a horizontal line at a distance 15 m above the load in a full-space for a Poisson's ratio of (a) 0.49; (b) 0.33.

4.2 Results in a circle around the excitation

To investigate the mechanism behind this phenomenon, Figure 8 shows the response at locations in a circle with radius 15 m from the load. The results are shown normalised to the maximum value of the pseudo-resultant at the frequency in question. These results are for a Poisson's ratio of 0.49, i.e. a compressional wave speed of 1570 m/s. The results at larger (or smaller) distances are identical to those at this distance but at correspondingly higher (or lower) frequencies. At low frequency (or short distance) the vibration is strongest above the load whereas at higher frequency (or larger distance) the response above the load becomes much smaller than that to the side.

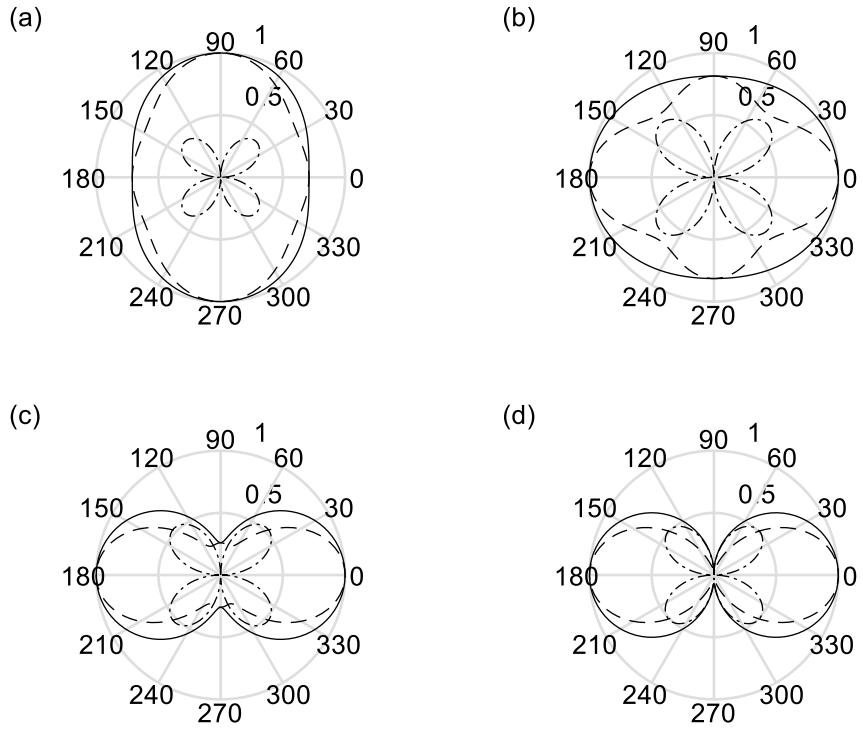

Figure 8. Pseudo-resultant normalised to maximum value and individual components for receivers at a distance 15 m from the load for a Poisson's ratio of 0.49. —, pseudo-resultant; – –, vertical; – · –, lateral. (a) 4 Hz, (b) 8 Hz, (c) 16 Hz, (d) 63 Hz.

Also shown in Figure 8 are the vertical and lateral components. The lateral component has a quadrupole-type directivity, being zero in both the vertical and lateral directions. These results can be interpreted in terms of the fundamental wave types. Directly above the load the response is due to compressional waves and is in the vertical direction whereas to the side the response is due to shear waves and again consists of vertical motion. The compressional motion is mostly limited to the nearfield region close to the excitation, i.e. for small distances or low frequencies. Thus, at low frequencies or a small distance from the excitation, the responses are dominated by the compressional wave. The maximum response occurs directly above excitation, as shown in Figure 8(a). With increase of frequency or the distance to the excitation, the compressional wave is attenuated rapidly while the shear wave dominates. The response at positions above the load reduces and the maximum responses occur at locations beside the load, thereby resulting in a shadow zone.

Figure 9 shows the corresponding results for a Poisson's ratio of 0.33, i.e. a compressional wave speed of 440 m/s. These show similar behaviour except that there is a larger component of the compressional wave so that the response above the load is larger at higher frequencies.

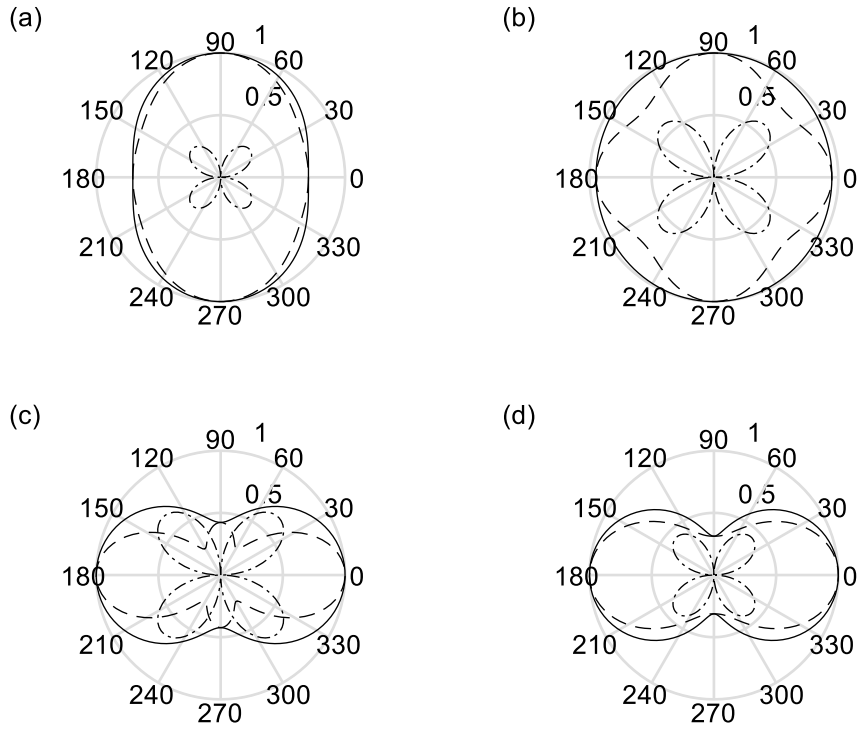

Figure 9. Pseudo-resultant normalised to maximum value and individual components for receivers at a distance 15 m from the load for a Poisson's ratio of 0.33. —, pseudo-resultant; – –, vertical; – · –, lateral. (a) 4 Hz, (b) 8 Hz, (c) 16 Hz, (d) 63 Hz.

5 The characteristics of the shadow effect for a half-space in the absence of a tunnel

As indicated in Section 4, the ground responses observed for a full-space without a tunnel exhibit some common features with the case of a tunnel in a half-space shown in Section 3. In this section the characteristics of the shadow effect in a half-space in the absence of a tunnel will be studied using a semi-analytical model before returning to the case with the tunnel in the next section.

5.1 The semi-analytical half-space ground model

A semi-analytical layered ground model, based on the formulation of Kausel and Roësset [28], is used here to study the shadow effect on the ground surface due to a point force excitation in the ground at a certain depth. In this model, the ground is represented by the stiffness matrices of various layers expressed in the wavenumber domain. The model is considered to be axisymmetric. Again, the horizontal axis is taken as y and the vertical axis as z, where z=0 is the free surface and z<0 is the half-space. Although the ground is assumed to be homogeneous, an interface between two soil layers is introduced at the location of the

force. However, the soil properties beneath and above the interface are kept the same. The unit force is applied over a circular area of diameter 0.6 m (the size of the excitation area has no effect on the responses in the far field). The displacements at the ground surface are monitored at distances from 0 to 40 m with a spacing of 0.5 m. The soil properties used in the ground model are initially based on the parameters for London clay, as shown in Table 2.

Based on the semi-analytical half-space model, the vertical and lateral transfer receptances on the ground surface are determined. The pseudo-resultant responses at four different frequencies are plotted against the lateral distance y from the excitation in Figure 10. The excitation is applied at the ground surface (at 0 m) and at depth of 15 m.

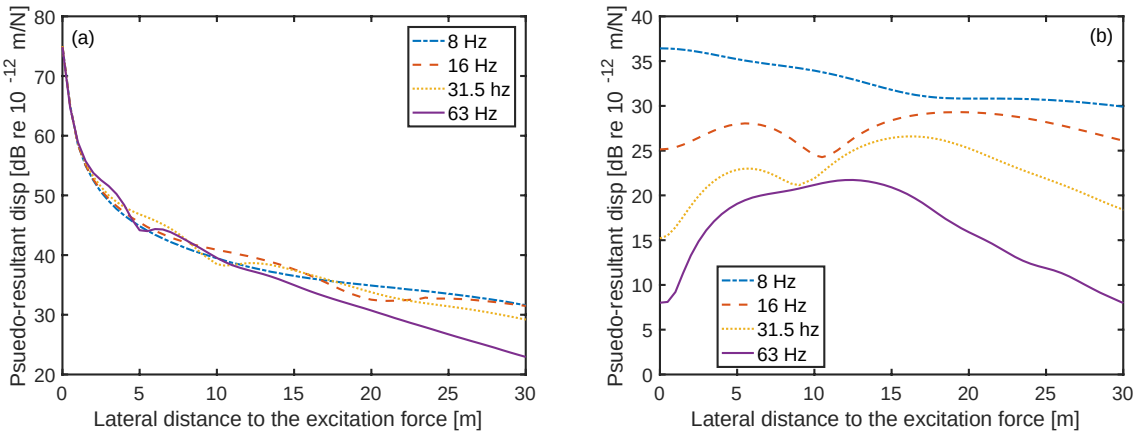

Figure 10. Displacements on the ground surface in different frequency bands due to excitation at depth of (a) 0 m, (b) 15 m.

It is shown in Figure 10(a) that, for the excitation at the ground surface, the peak response occurs at the force location (y=0) for all the example frequencies. For the excitation at 15 m depth, as shown in Figure 10(b), the distribution of vibration has strong similarities to those shown in Figure 5 and Figure 7 for the case with the tunnel and the full-space. This shows that the shadow effect exists in the half-space when the excitation is at certain depth in the soil. Compared with the full-space results, the results for the half-space are closer to those for the tunnel case, due to the influence of the free surface.

5.2 Influence of excitation depth

With a unit vertical force applied at different depths, the spectra of the pseudo-resultant responses on the ground surface are plotted in Figure 11. The excitation is applied at different depths of 5, 10 and 15 m in the ground. The response levels on the ground surface directly above the excitation (at y=0), shown in thick lines, reduce when the force is moved deeper into the ground and drop rapidly at higher frequencies. This is due to the decay of the

compressional wave component, as indicated in Section 4.2. Also shown in thin lines are the maximum values over the ground surface at each frequency. The cut-on frequency, above which the maximum responses start to move away from y=0, reduces as the depth is increased.

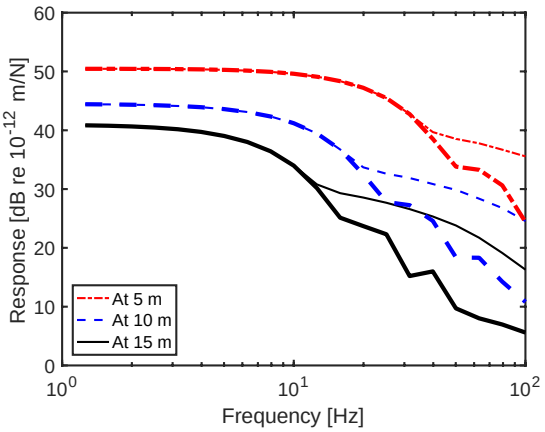

Figure 11. Pseudo-resultant response on the ground surface plotted against frequency compared for forces at different depth (5, 10 and 15 m): thick lines: directly above the excitation (at y=0); thin lines: maximum response.

The magnitude of the shadow effect, which is the level difference in dB between the result at y=0 and maximum value, is plotted in Figure 12(a). Figure 12(b) shows the width of the shadow zone, normalised by the depth. Both results are plotted against a non-dimensional frequency expressed as fd/c_s where f is frequency, d is depth of the excitation point and c_s is the shear wave speed. This corresponds to the ratio of the depth to the shear wavelength in the soil. The results from the three depths collapse to a single curve when plotted in this form.

The cut-on frequency can be clearly identified at the point when $fd/c_s = 1$. As the shear wave speed is constant in this case, the cut-on frequency is inversely proportional to the excitation depth. Above the cut-on frequency (i.e. for $fd/c_s > 1$), the magnitude of the shadow effect increases approximately as $20\log_{10}(fd/c_s)$, as shown in Figure 12(a); the normalised width of the shadow area, as shown in Figure 12(b), reduces approximately as $-1.5\log_{10}(fd/c_s)$. For the same frequency, as the excitation becomes deeper, the shadow zone becomes larger and wider.

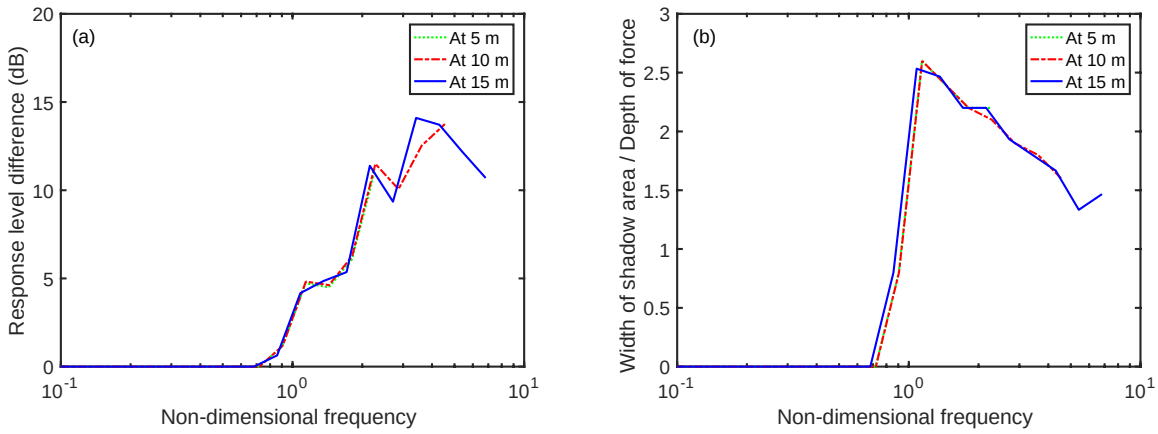

(a) (b)

Figure 12. Response level difference (a) and width of shadow area (b) plotted against non-dimensional frequency fd/c_s compared for force at different depths.

5.3 Influence of shear wave speed

In this section results are shown for cases with different shear wave speeds (c_s). As well as the material considered above, for which c_s = 220 m/s, results are shown for two nominal grounds in which c_s is halved to 110 m/s or doubled to 440 m/s, while the compressional speed is kept constant as 1570 m/s.

Figure 13 shows the spectra of responses on the ground surface due to the excitation at a depth of 15 m. At low frequencies, both the response level at y=0 and the maximum response level become larger with the reduction of c_s in the soil. However, at higher frequencies the responses above the excitation point reduce rapidly, especially for the case with a low soil shear wave speed.

The magnitude and width of the shadow zone are plotted against the non-dimensional frequency in Figure 14. Similar to Figure 12, the cut-on of the shadow effect occurs at a non-dimensional frequency of unity in each case, indicating that the cut-on frequency is proportional to c_s. Above the cut-on frequency, the magnitude of the shadow effectincreases with frequency, as shown in Figure 14(a), while the width of the shadow zone decreases, as shown in Figure 14(b), similar to those in Figure 12.

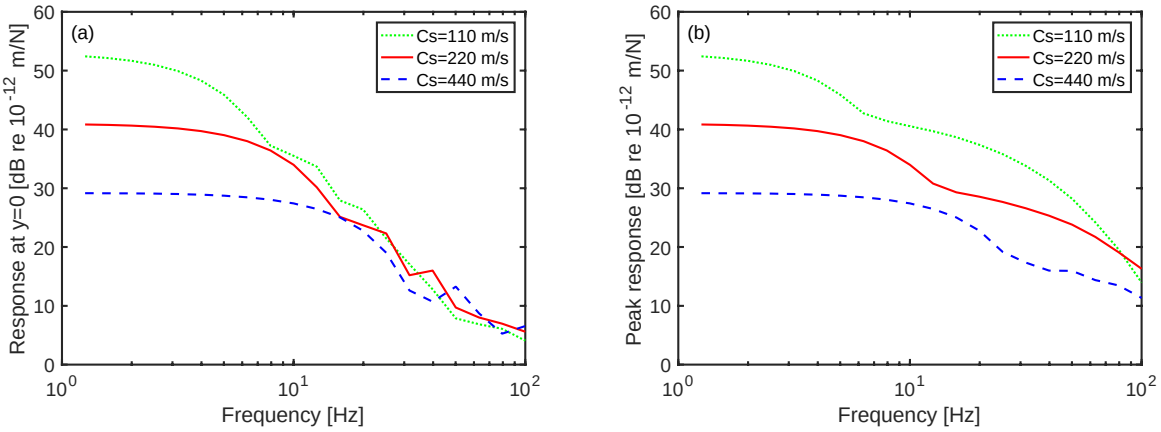

Figure 13. Response at y=0 (a) and maximum response (b) plotted against frequency for different soil shear wave speeds; depth of force 15 m.

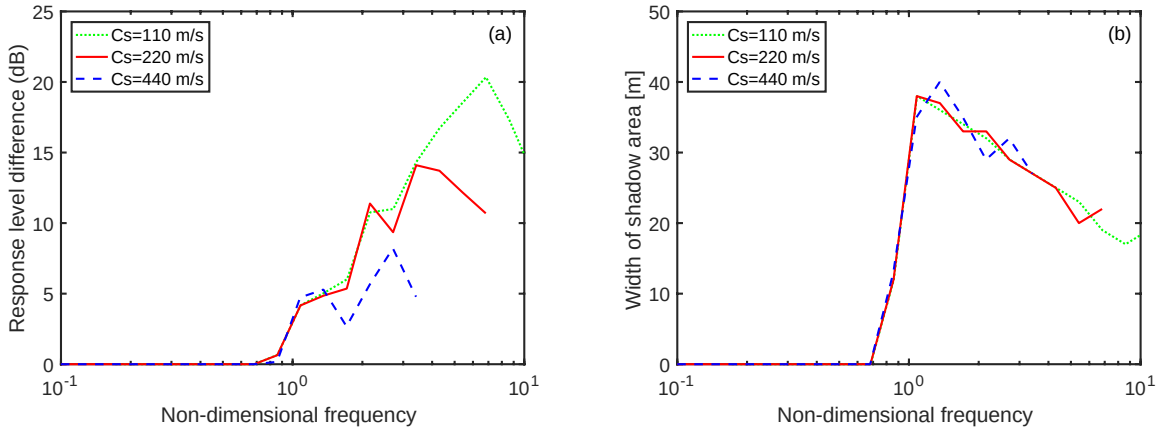

Figure 14. Response level difference (a) and width of shadow area (b) plotted against non-dimensional frequency fd/c_s for different soil shear wave speeds; depth of force 15 m.

5.4 Influence of compressional wave speed

Results are compared for three cases to examine the effect of varying the compressional wave speed (c_p). The responses on the ground surface to a vertical excitation at 15 m below the ground surface are again shown in each case. Three values of c_p are used for the soil, which are 1570 (as used previously), 1000 and 660 m/s while the shear wave speed is kept constant as 220 m/s. This is achieved by setting the Poisson's ratio to 0.49, 0.47 and 0.44 and keeping the shear modulus constant.

The responses directly above the excitation force (y=0) are plotted in Figure 15(a) against frequency. Below 10 Hz the responses at y=0 are only slightly influenced by the variation of c_p. Above 10 Hz (the cut-on frequency in this case), the response with a lower value of c_p is higher, as seen for the full-space in Section 4. Figure 15(b) shows the maximum responses on

the ground surface at each frequency. The variation of c_p has very little influence on the amplitude of the maximum response for the whole frequency range.

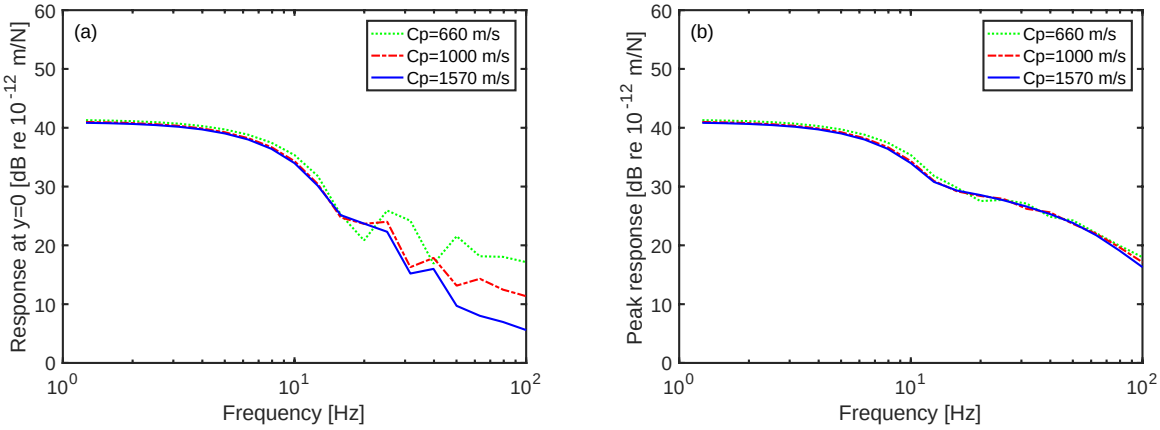

Figure 15. Pseudo-resultant response: (a) at y=0 and (b) maximum response, plotted against frequency for different soil compressional wave speeds; depth of force 15 m.

The level difference between the maximum responses and those directly above the force, i.e. the magnitude of the shadow effect, is plotted in Figure 16(a). It can be seen that the cut-on frequency is unaffected by the compressional wave speed. Above this frequency, which is 10 Hz for all values of c_p, the magnitude of shadow effectis initially the same in each case but at higher frequency this level difference is greater for the cases with larger values of c_p. It also shows a tendency to decrease after reaching a peak, which resembles those shown in Figure 14(a). According to the results in Figure 8 and Figure 9, it is the differences in Poisson's ratio that are responsible for the size of the level difference. The width of the shadow area is displayed against frequency in Figure 16(b). It is only slightly influenced by the compressional wave speed.

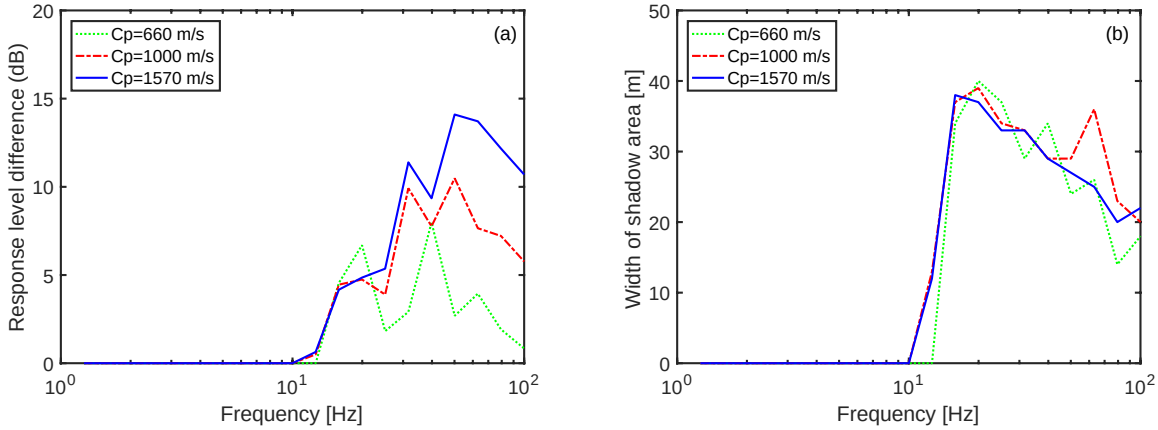

Figure 16. Response level difference (a) and width of shadow area (b), plotted against frequency for different soil compressional wave speeds; depth of force 15 m.

6 Influence of the existence of the tunnel structure

The features of the shadow effect in the half-space ground without the tunnel have been studied in the previous section. The vibration induced by a force acting on the tunnel base has similar features to that obtained by the ground model excited by a force at the same depth as the tunnel base. However, the presence of the tunnel structure will modify the shadow effect. Therefore, in this section, the results with and without the tunnel structure are compared and the influence from varying the tunnel parameters is studied.

6.1 Lined and unlined tunnel

To study the shadow effect in the ground vibration in the presence of a lined tunnel, the 2.5D FE/BE model described in Section 3.1 is used to calculate the responses on the ground surface to the excitation at the tunnel bottom. The soil and tunnel properties used in the model are the same as given in Table 2. In addition an unlined tunnel, i.e. a cavity without the tunnel structure, and a ground without the tunnel are considered. To represent the unlined tunnel, for simplicity the same 2.5D FE/BE model is used but with the material of the tunnel in the FE model replaced with that of the surrounding soil. The depth is 15 m from the ground surface to the tunnel centreline, 16.9 m to the excitation point. For the ground model without tunnel, the force is applied at the same depth as that in the tunnel-ground models, i.e. 16.9 m. For this case, the half-space ground is still modelled using the semi-analytical model, as described in Section 5.

Figure 17 shows the pseudo-resultant vibration on the ground surface due to a unit force for these three models. This confirms that the distributions of vibration on the ground surface for the cases with and without the tunnel structure are very similar, that is the maximum response occurs at some distance away from the excitation above a certain frequency.

At 8 Hz, the responses on the ground surface are the largest for the case without the tunnel. With the increase of frequency, the responses from all three models decrease. The reduction is greater above the excitation point (y=0) than at some distance away, leading to the formation of the shadow area. Moreover, within the shadow area, the responses from the model with the tunnel are higher than those from the model without the tunnel at high frequencies (31.5 and 63 Hz).

Although all three models show a shadow effect at higher frequencies, the magnitude and width of the shadow area are different for each case. The response level difference between the maximum response and that directly above the force is compared for the three cases in Figure 18(a). This is slightly enlarged in the presence of the tunnel structure. The widths of

the shadow area of the three cases are also plotted against frequency in Figure 18(b). It can be clearly seen that the shadow area is reduced in width by the presence of the lined or unlined tunnel. Moreover, the cut-on frequency with the lined tunnel is slightly lower than that without it.

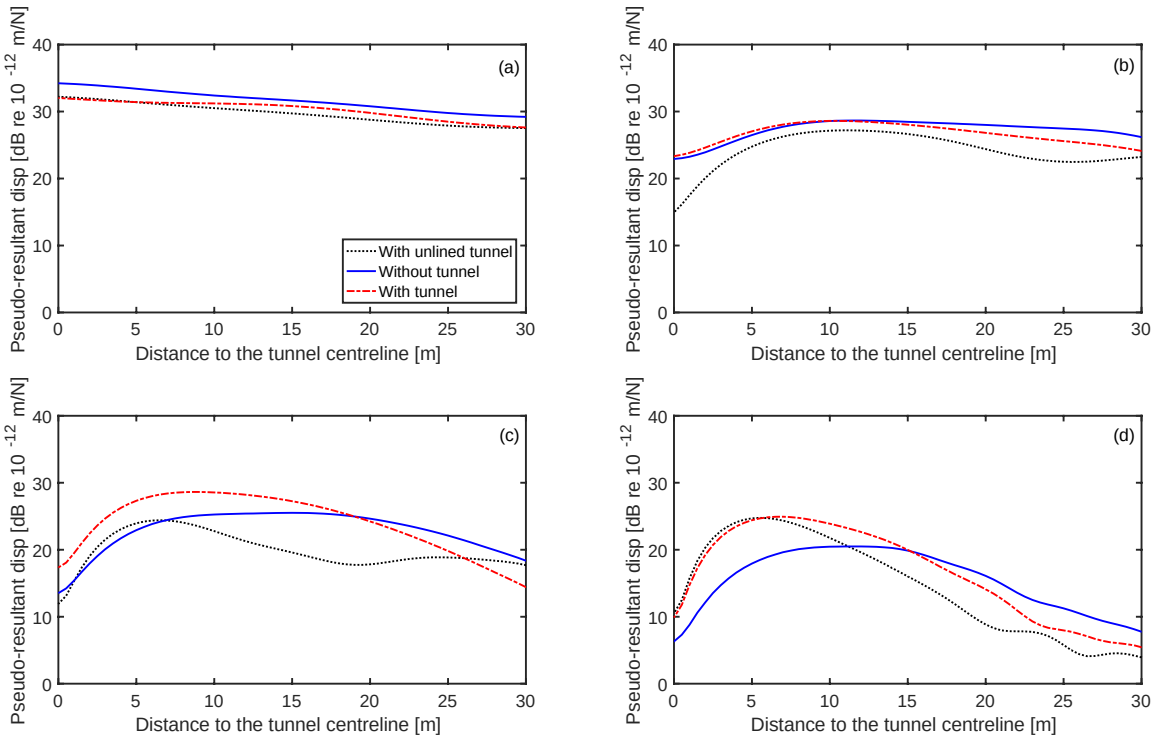

Figure 17. Pseudo-resultant displacement responses to a unit force compared at four excitation frequencies in one-third octave bands for three different models. (a) 8 Hz, (b) 16 Hz, (c) 31.5 Hz, (d) 63 Hz.

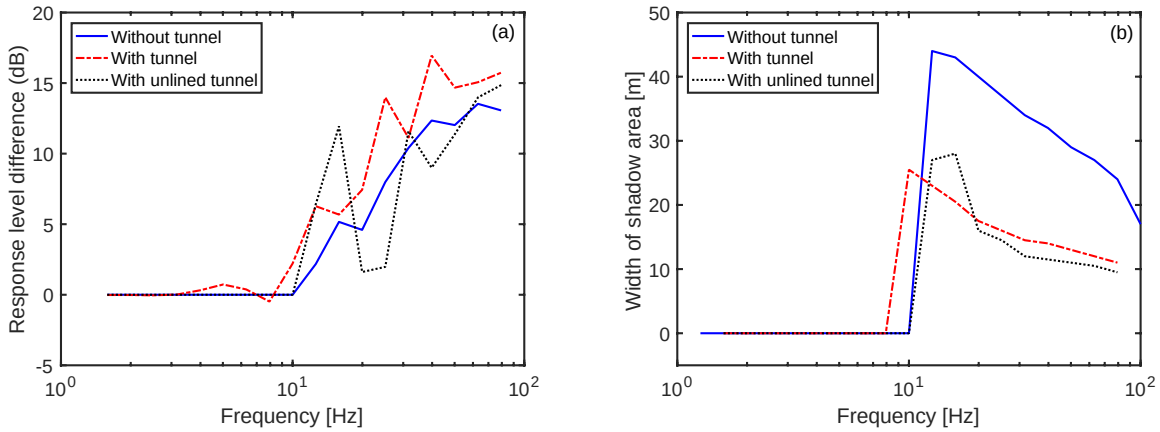

Figure 18. Response level difference (a) and width of shadow area (b) plotted against frequency for three different models.

It might be considered that the existence of the tunnel structure effectively raises the excitation point from the tunnel bottom to the crown, which would mean a reduction in the effective excitation depth. This would explain the reduction in shadow width after the introduction of the tunnel, as shown in Figure 18(b). However, according to the conclusions from the half-space ground model (Section 5), with a shallow excitation, the cut-on frequency will be higher, whereas the results in Figure 18 show the opposite trend.

6.2 Tunnel diameter

As shown in the previous section, the characteristics of the shadow effect differ not only between the models with and without the tunnel, but they also differ slightly between the lined and unlined tunnels. It can be expected that the tunnel diameter will also have an impact on the characteristics of the shadow effect.

The magnitude of the shadow effect, i.e. the ratio of the maximum response to that at y=0 m, is plotted in Figure 19(a) against frequency for the cases with two different tunnel diameters. The inner diameters of the tunnels are 3.81 and 5.675 m. For both tunnels, the lining thickness is 220 mm and the tunnel depth is now 25 m from the ground surface to the tunnel centre. It shows that the variation of tunnel diameter has little influence on the shadow depth. The width of the shadow area is shown in Figure 19(b) for different tunnel diameters. These results show that the cut-on frequency of the smaller tunnel is slightly higher than that of the larger tunnel, and its shadow zone is slightly wider at a given frequency.

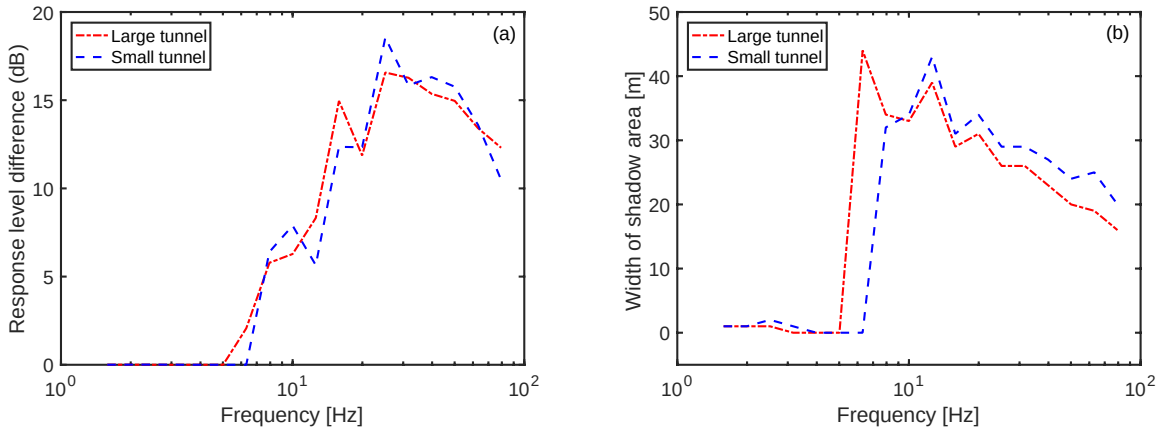

Figure 19. Response level difference (a) and width of shadow area (b), plotted against frequency for different tunnel diameters. Depth of tunnel 25 m.

6.3 Lining thickness

Figure 20 shows the influence of the tunnel lining thickness on both the magnitude and width of the shadow area on the ground surface. In these examples, the tunnels have the same

inner diameter, which is 3.81 m, while the outer diameter is varied to give different lining thicknesses. The tunnel depth is again 25 m. It can be seen that the lining thickness has a negligible impact on the shadow effect at the ground surface.

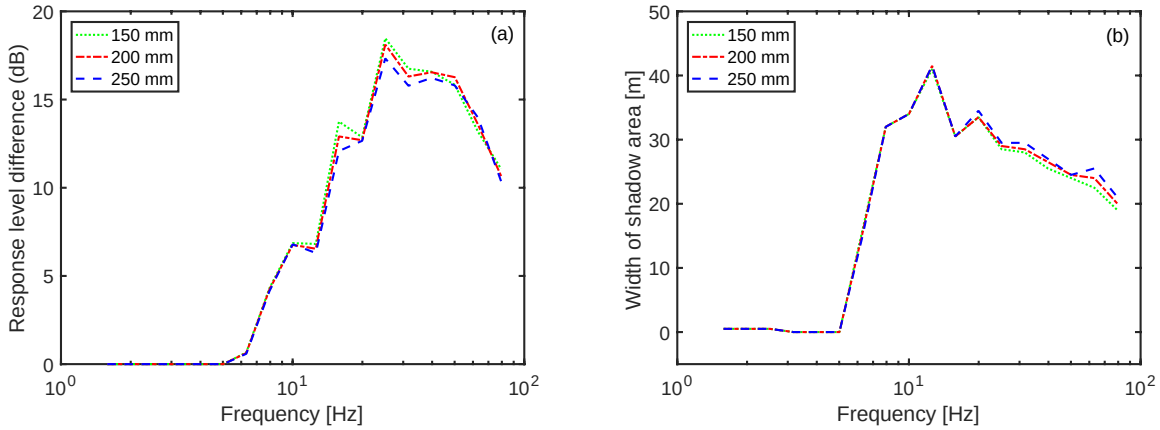

Figure 20. Response level difference (a) and width of shadow area (b), plotted against frequency for different lining thicknesses. Depth of tunnel 25 m.

7 Conclusions

In this study of vibration at the ground surface above a tunnel, it has been shown that the maximum vibration occurs at some distance from the tunnel centreline for frequencies above a certain value. The vibration directly above the tunnel is up to 15 dB lower than the maximum levels at a lateral distance. This appears like a shadow effect. Similar results have been found in measurements taken at a location above a tunnel on a high-speed railway line. This phenomenon is found to be an effect of the propagation of the fundamental waves in the soil, which exists in any homogeneous elastic medium including a full-space and a half-space.

According to the results from a full-space model, the compressional wave motion, which dominates the response directly above the excitation, is limited to the nearfield close to the excitation. The cut-on frequency, above which the maximum response no longer occurs directly above the excitation force, can be interpreted in terms of the transition from near-field behaviour to far-field behaviour for a force acting on an elastic medium. Away from the centreline of the excitation, the shear waves play an important role in determining the vibration levels. The soil shear wave speed therefore has a greater impact on the shadow area behaviour than the compressional wave speed.

Based on a semi-analytical ground model where a free surface is incorporated, the influence of the excitation depth and the soil properties on the shadow effect has been

studied. The cut-on frequency is found to be proportional to the shear wave speed and inversely proportional to the depth of the excitation force in the soil. Above the cut-on frequency, a shadow zone is formed so that the vibration level is lower above the excitation than at some distance away. The width of the shadow zone and the maximum level difference within it are both functions of a non-dimensional frequency which corresponds to the ratio of the excitation depth to the shear wavelength in the soil. For a deeper excitation, the shadow zone becomes wider and the level difference is larger. The width and magnitude of the shadow zone both decrease with the increase of the soil shear wave speed. For a given excitation depth and shear wave speed, the shadow width decreases with the frequency while the maximum level difference first increases and then decreases after reaching a maximum. The influence from the compressional wave on the three characteristics of the shadow effect is less significant. However, with a higher compressional wave speed, or a higher Poisson's ratio, the maximum level difference is larger.

A 2.5D FE/BE model has been used to represent the coupled tunnel-ground situation. When the tunnel is present the vibration on the ground surface caused by excitation at the tunnel base shares many of the features found in the absence of the tunnel. However, due to the presence of tunnel, the vibration level within the shadow area is increased at high frequencies, and the width of the shadow zone is significantly reduced. The diameter and thickness of the tunnel have no significant influence on the features of the shadow area. The shape of the tunnel and the presence of soil layering may also affect the shadow effect, but these are beyond the scope of the current study.

All data published in this paper are openly available from the University of Southampton repository at https://doi.org/10.5258/SOTON/D1242 .

References

[1] Lombaert G, Degrande G, François S, Thompson DJ. Ground-borne vibration due to railway traffic: A review of excitation mechanisms, prediction methods and mitigation measures. Noise Vib Mitig Rail Transp 2015;126:253–87. https://doi.org/10.1007/978-3-662-44832-8_33.

[2] Thompson DJ, Kouroussis G, Ntotsios E. Modelling, simulation and evaluation of ground vibration caused by rail vehicles. Veh Syst Dyn 2019;57:936–83. https://doi.org/10.1080/00423114.2019.1602274.

[3] Connolly DP, Marecki GP, Kouroussis G, Thalassinakis I, Woodward PK. The growth

of railway ground vibration problems — A review. Sci Total Environ 2016;568:1276–82. https://doi.org/10.1016/j.scitotenv.2015.09.101.

[4] Sheng X. A review on modelling ground vibrations generated by underground trains. Int J Rail Transp 2019:241–61. https://doi.org/10.1080/23248378.2019.1591312

[5] Gutowski TG, Dym CL. Propagation of ground vibration: A review. J Sound Vib 1976;49:179–93. https://doi.org/10.1016/0022-460X(76)90495-8.

[6] Thompson DJ. Railway noise and vibration: mechanisms, modelling and means of control. Elsevier: Oxford; 2008.

[7] Kuppelwieser H, Ziegler A. A tool for predicting vibration and structure-borne noise immissions caused by railways. J Sound Vib 1996;193:261–7. https://doi.org/10.1006/jsvi.1996.0266.

[8] Madshus C, Bessason B, Hårvik L. Prediction model for low frequency vibration from high speed railways on soft ground. J Sound Vib 1996;193:195–203. https://doi.org/10.1006/jsvi.1996.0259.

[9] Hood RA, Greer RJ, Breslin M, Williams PR. The calculation and assessment of ground-borne noise and perceptible vibration from trains in tunnels. J Sound Vib 1996;193:215–25. https://doi.org/10.1006/jsvi.1996.0261.

[10] Hanson C, Towers D, Meister L. Transit Noise and Vibration Impact Assessment, Report FTA-VA-90-1003-06. 2006.

[11] Forrest JA, Hunt HEM. A three-dimensional tunnel model for calculation of train-induced ground vibration. J Sound Vib 2006;294:678–705. https://doi.org/10.1016/j.jsv.2005.12.032.

[12] Forrest JA, Hunt HEM. Ground vibration generated by trains in underground tunnels. J Sound Vib 2006;294:706–36. https://doi.org/10.1016/j.jsv.2005.12.031.

[13] Kuo KA, Hunt HEM, Hussein MFM. The effects of a second tunnel on the propagation of ground-borne vibration from an underground railway. J Sound Vib 2011;330:6203–22. https://doi.org/10.1007/978-4-431-53927-8_36.

[14] Sheng X, Jones CJC, Thompson DJ. Ground vibration generated by a harmonic load moving in a circular tunnel in a layered ground. J Low Freq Noise Vib Act Control 2003;22:83–96. https://doi.org/10.1260/026309203322770338.

[15] Jones CJC, Thompson DJ, Petyt M. A model for ground vibration from railway tunnels. Proc Inst Civ Eng Transp 2002;153:121–9. https://doi.org/10.1680/tran.2002.153.2.121.

[16] Sheng X, Jones CJC, Thompson DJ. Modelling ground vibration from railways using wavenumber finite- and boundary-element methods. Proc R Soc A Math Phys Eng Sci 2005;461:2043–70. https://doi.org/10.1098/rspa.2005.1450.

[17] Clouteau D, Arnst M, Al-Hussaini TM, Degrande G. Freefield vibrations due to dynamic loading on a tunnel embedded in a stratified medium. J Sound Vib 2005;283:173–99. https://doi.org/10.1016/j.jsv.2004.04.010.

[18] Degrande G, Clouteau D, Othman R, Arnst M, Chebli H, Klein R, et al. A numerical model for ground-borne vibrations from underground railway traffic based on a periodic finite element-boundary element formulation. J Sound Vib 2006;293:645–66. https://doi.org/10.1016/j.jsv.2005.12.023.

[19] Ding DY, Gupta S, Liu WN, Lombaert G, Degrande G. Prediction of vibrations induced by trains on line 8 of Beijing metro. J Zhejiang Univ Sci A 2010;11:280–93. https://doi.org/10.1631/jzus.A0900304.

[20] Gupta S, Stanus Y, Lombaert G, Degrande G. Influence of tunnel and soil parameters on vibrations from underground railways. J Sound Vib 2009;327:70–91. https://doi.org/10.1016/j.jsv.2009.05.029.

[21] Yang YB, Hung HH. Soil vibrations caused by underground moving trains. J Geotech Geoenvironmental Eng 2008;134:1633–44. https://doi.org/10.1061/(ASCE)1090-0241(2008)134:11(1633).

[22] Galvín P, François S, Schevenels M, Bongini E, Degrande G, Lombaert G. A 2.5D coupled FE-BE model for the prediction of railway induced vibrations. Soil Dyn Earthq Eng 2010;30:1500–12. https://doi.org/10.1016/j.soildyn.2010.07.001.

[23] Lopes P, Costa PA, Ferraz M, Calçada R, Cardoso AS. Numerical modeling of vibrations induced by railway traffic in tunnels: From the source to the nearby buildings. Soil Dyn Earthq Eng 2014;61:269–85. https://doi.org/10.1016/j.soildyn.2014.02.013.

[24] Nilsson C-M, Jones CJC. Theory Manual for WANDS 2.1: Wave-Number-Domain FE-BE Software for structures and fluids. ISVR Technical Memorandum No. 975, University of Southampton UK 2007.

[25] Jin Q, Thompson DJ. Study of the shadow effect caused by a railway tunnel. J. Phys.

Conf. Ser., vol. 744, 2016, p. 012143. https://doi.org/10.1088/1742-6596/744/1/012143.

[26] Jin Q, Thompson DJ, Lurcock DEJ, Toward MGR, Ntotsios E. A 2.5D finite element and boundary element model for the ground vibration from trains in tunnels and validation using measurement data. J Sound Vib 2018;422:373–89. https://doi.org/10.1016/j.jsv.2018.02.019.

[27] Kausel E. Fundamental Solutions in Elastodynamics. Cambridge University Press; 2006. https://doi.org/10.1017/cbo9780511546112.

[28] Kausel E, Roësset JM. Stiffness matrices for layered soils. Bull Seismol Soc Am 1981;71:1743–61. https://doi.org/10.1016/0148-9062(83)91665-0.